Effect of Hydrogen-Bonding Complexation on the Interfacial Behavior of Poly(isoprene)−*b*-Poly(ethylene oxide) and Poly(isoprene)−*b*-Poly(acrylic acid) Langmuir Monolayers

Dinghai Xie,[†,‡] Camila A. Rezende,[‡] Guangming Liu,[†] Stergios Pispas,[§] Guangzhao Zhang,[†] and Lay-Theng Lee*[,‡]

The Hefei National Laboratory for Physical Sciences at Microscale and Department of Chemical Physics, University of Science and Technology of China, Hefei, Anhui 230026, China, Laboratoire Léon Brillouin, UMR12, CEA-Saclay, 91191 Gif-sur-Yvette Cedex, France, and Theoretical and Physical Chemistry Institute, National Hellenic Research Foundation, 48 Vassileos Constantinou Avenue, 11635 Athens, Greece

Received: October 6, 2008; Revised Manuscript Received: November 20, 2008

The effect of hydrogen-bonding complexation on the interfacial behavior of poly(isoprene)−*b*-poly(ethylene oxide) (PI−*b*-PEO) diblock copolymer at the air−water interface has been investigated by Langmuir balance and neutron reflectivity. PI−*b*-PEO forms Langmuir monolayers with PI as the anchoring block. Introduction of a second diblock, poly(isoprene)−*b*-poly(acrylic acid) (PI−*b*-PAA) yields PI−*b*-PEO/PI−*b*-PAA mixed layers with interfacial behavior that is pH-dependent. At pH 10.0 and 5.7, the compression ($\pi-A$) isotherms exhibit three regions that are characteristic of PEO-type tethered layers, (i) a low-pressure 2-D "pancake" region (region I), (ii) a pseudoplateau where PEO segments desorb and are immerse in the subphase (region II), and (iii) a steep pressure rise region commonly considered as the "brush" regime (region III). At pH 2.5, on the other hand, the $\pi-A$ isotherm shows only two regions, (I) and (III). This novel behavior is attributed to hydrogen-bonding complexation between the undissociated carboxylic acids and the PEO, forming very compact layers. It appears that desorption of PEO segments is hindered as a consequence of this complexation. Furthermore, no brush-like structure is observed in region III of the isotherml; thus, the steep rise in surface pressure in this case arises primarily from interactions of the anchoring block. The hydrogen-bonded complex of PI−*b*-PEO/PI−*b*-PAA monolayers thus shows enhanced surface stability.

Introduction

Polymer chains attached by one end to an interface show interesting properties and have been extensively investigated.[1−13] Among them, amphiphilic diblock copolymers have been exploited to control interfacial properties at the air−water interface, where a hydrophobic block anchors the hydrophilic soluble block to the free surface. Most of the investigations are focused on poly(ethylene oxide) (PEO) diblock copolymers mainly because PEO absorbs weakly to the air−water interface and it is biocompatible.[14−27] Using the Langmuir balance technique, Bijsterbosch et al. revealed that the surface pressure−area ($\pi-A$) isotherms exhibit three regions with increasing coverage, namely, a region where the PEO adsorbs in a 2-D "pancake" structure (low surface coverage), a pseudoplateau region where adsorbed PEO segments desorb from the interface and immerse into the subphase (intermediate coverage), and a "brush" region consisting of stretched chains (high coverage) where the surface pressure increases sharply.[14] Gonçalves da Silva et al. also proposed that a pseudoplateau at surface pressure near 10 mN/m may be associated with dissolution of the PEO chains into the water subphase to form a quasi-brush.[15] On the other hand, Lennox et al. showed that the PEO block may initially undergo a dehydration process followed by a conformational change upon compression instead of immersing into the aqueous subphase to form a brush.[20] Thus, the interfacial behavior of amphiphilic diblock copolymers upon compression is still not completely understood and remains a topic of interest.

It is known that poly(acrylic acid) (PAA) exhibits a pH-induced conformational transition and can form complexation with poly(ethylene oxide) (PEO) by hydrogen bonding.[28] Mixed monolayers of such diblock copolymers capable of forming hydrogen bonds thus provide an interesting system to probe potential novel interfacial properties.[29] Regen et al. suggested that charged surfactant monolayers, when cross-linked ionically with polymeric counterions, provide a strategy for forming Langmuir−Blodgett (LB) films bearing good gas permeability and stability properties.[30−33]

In the present study, we investigate the effect of hydrogen-bonding complexation on the interfacial behavior of Langmuir monolayers consisting of PI−*b*-PEO and PI−*b*-PAA diblock copolymers. Here, the PI acts as an anchoring block for the PEO and the PAA. In contrast to polystyrene (PS), which is commonly used as anchoring block, PI has a low T_g (≈-68 °C) that facilitates spreading, and equilibrium can be reached more easily especially at high surface pressures.[34] Using the Langmuir balance technique coupled with neutron reflectivity, we explore the interfacial behavior of these PI−*b*-PEO and PI−*b*-PAA mixed layers. The effects of pH and of hydrogen-bonding complexation on the structure and the stability of the mixed layers are investigated. We show that hydrogen -bonding complexation leads to formation of compact surface layers with a novel interfacial behavior.

* To whom correspondence should be addressed. E-mail: Lay-Theng.Lee@cea.fr.
[†] University of Science and Technology of China.
[‡] Laboratoire Léon Brillouin, UMR12.
[§] National Hellenic Research Foundation.

10.1021/jp808821s CCC: $40.75
Published on Web 12/30/2008

Experimental Section

Materials. The PI−*b*-PEO and PI−*b*-PAA diblock copolymers were synthesized via anionic polymerization.[35] The molecular weight (M_w) and the polydispersity (M_w/M_n) of PI−*b*-PEO and PI−*b*-PAA were characterized by a combination of gel permeation chromatography (GPC) and NMR. For PI_{92}−*b*-PEO_{1290} and PI_{63}−*b*-PAA_{530}, $M_w/M_n = 1.03$ and 1.16, respectively.

PI−*b*-PEO solution was prepared by dissolving the sample in chloroform directly, and PI−*b*-PAA solution was prepared in $CHCl_3/CH_3OH$ (1/1, v/v). The mixture of the PI−*b*-PEO/PI−*b*-PAA solution was made by dissolving the mixture in $CHCl_3/CH_3OH$ (1/1, v/v) at molar ratio of EO/AA units ∼ 1. The concentration of all of the solutions was 1.0×10^{-3}g/mL.

Surface Pressure Measurements. Surface pressure−area isotherms were recorded using a Kibron MicroTroughX (Kibron Inc., Finland). All experiments were conducted at 20 °C. The trough area was 108 cm^2, and the trough volume was ∼22 mL. The water used in the subphase was purified with the Millipore Milli-Q system, where the resistivity is 18.2 MΩ·cm and the pH is 5.7. The pH of the subphase was adjusted to pH 10.0 and 2.5 by NaOH and HCl solutions, respectively. The diblock polymer solution was spread on the water surface with a 10 μL Hamilton microliter syringe. After complete evaporation of the solvent (∼30 min), the surface film was compressed symmetrically at a constant speed of 5 mm/min. The surface pressure isotherms were recorded in real time with a Wilhelmy wire probe. Several compression−expansion cycles were performed for each sample.

Neutron Reflectometry. Neutron reflectivity experiments were carried out on the time-of-flight reflectometer EROS (Laboratoire Léon Brillouin, CEA-Saclay, France). The spectra were acquired on monolayers prepared in the Kibron MicroTroughX trough. The plastic cover of the trough was fitted with quartz windows to allow the neutron beam to enter and exit the trough with minimal absorption. Special care was taken to seal the trough to minimize the exchange of water vapor with the deuterated subphase. We used a subphase consisting of a mixture of D_2O/H_2O (80/20 v/v). The scattering length density of this solvent was $Nb_s = 4.68 \times 10^{-6}$ $Å^{-2}$. We find that by using this mixture, the degree of change in the scattering length density of the subphase (due to exchange with the atmosphere) at the end of the measurements is reduced to less than 5%, compared to about 10% for pure D_2O. The grazing incident angle was $\theta = 1.55°$, and the angular solution was $\delta\theta \approx 3\%$. The wavelengths range from $\lambda \approx 3$ to 22 Å, corresponding to wave vector $k = (2\pi)/(\lambda)\sin\theta$ ranging from 0.005 to 0.06. The required volume of the diblock polymer solution was spread on the surface of the subphase that was preadjusted to the desired pH. After about 30 min, the monolayer was compressed to the desired surface pressure, and neutron reflectivity spectra were acquired at 1 h intervals. In all cases, no kinetics effects were observed, and the spectra were summed for improved statistics.

Results and Discussions

Surface Pressure Measurements. ***(i) PI−b-PEO Monolayers.*** Figure 1 shows the compression isotherms for the diblock copolymer, PI_{92}−*b*-PEO_{1290} spread on the surface of water at different pHs. In this figure, the surface pressure is plotted as a function of area per molecule of the PEO block. It can be seen that from pH 2.5 to 10.0, the isotherms almost superpose, showing that pH does not have a significant effect on the monolayers. These isotherms show a slow rise in pressure followed by a pseudoplateau region, the onset of which occurs at ∼10.5 mN/m, a value that corresponds to the saturation pressure of adsorbed PEO homopolymer. These two distinct regions are consistent with those observed for PEO homopolymers.[14] The region of slow pressure rise is ascribed to 2-D segment interactions. This "pancake" region (region I) and the onset of the pseudoplateau are thus independent of polymer chain length, and isotherms for different chain lengths superpose when plotted versus area per EO monomer (results not shown). Extrapolation of the pancake region of the isotherm to $\pi = 0$ yields the pancake limiting area, $A_{pancake} \approx 352.0$ nm^2. This gives an average area per EO monomer of ∼0.27 nm^2, in good agreement with the previous studies.[15] In the pseudoplateau region, steric repulsion of the PEO chains exceeds attractive interaction between the PEO and the air−water interface, and the polymer segments gradually desorb from the interface and immerse into the subphase. The onset of this crossover takes place at the EO monomer area of ∼0.12 nm^2. The gradual rise in pressure in the pseudoplateau is indicative of conformational changes, more apparent in this case compared to that for the homopolymer, due to the PI anchoring block preventing complete dissolution of the molecule into the subphase. Thus, for the range of surface coverages studied, the interfacial behavior of the spread PI_{92}−*b*-PEO_{1290} is dominated by the PEO block.

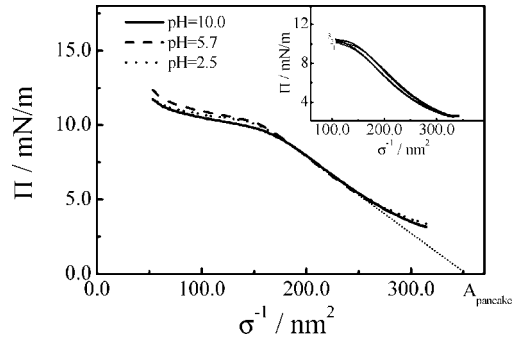

Figure 1. Surface pressure versus area per molecule for the PI_{92}−*b*-PEO_{1290} diblock copolymer at different pHs.

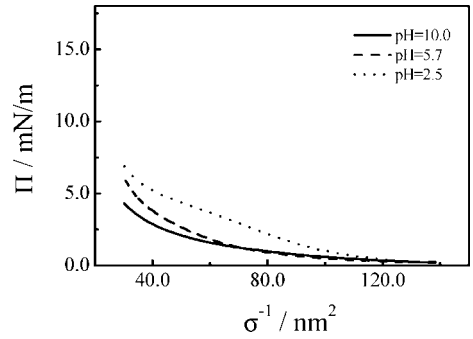

Figure 2. Surface pressure versus area per molecule for PI_{63}−*b*-PAA_{530} diblock copolymer at different pHs.

The inset in Figure 1 shows three compression−expansion cycles of surface pressure isotherms conducted within the pseudoplateau region (target area per molecule = 110 nm^2) at pH 5.7. A reproducible hysteresis is observed in all compression−expansion cycles; this hysteresis is commonly attributed to chain entanglement during compression and a time lag for disentanglement during decompression.

(ii) PI−b-PAA Monolayers. The π−*A* isotherms for the PI_{63}−*b*-PAA_{530} diblock copolymer at different pHs are given in Figure 2. PAA is a weak polyanion, and its ionization degree is strongly pH-dependent, with a pK_a of PAA of ∼5.6.[29] At pH 10.0, most of the carboxyl acid groups are deprotonated, and the charged PAA chains are hydrophilic and nonsurface active.

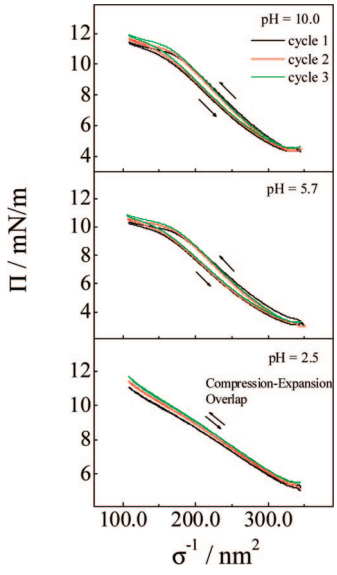

Figure 3. Compression isotherms for mixtures PI_{92}−*b*-PEO_{1290}/PI_{63}−*b*-PAA_{530} at low to intermediate surface coverage. Reproducible hysteresis is obtained for pH 10.0 and 5.7; for pH 2.5, compression and expansion curves overlap.

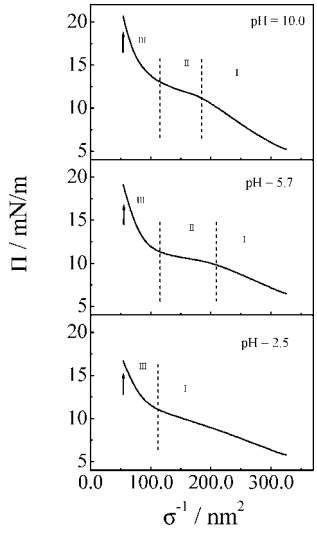

Figure 4. Compression isotherms for mixtures PI_{92}−*b*-PEO_{1290}/PI_{63}−*b*-PAA_{530} at high surface coverage. (Vertical arrows indicate the regions where neutron reflectivity measurements are taken.)

TABLE 1: Pancake Limiting Area ($A_{pancake}$) and "Brush" Limiting Area (A_{brush}) Obtained from Compression Isotherms for the Mixture of PI_{92}−*b*-PEO_{1290}/PI_{63}−*b*-PAA_{530}

sample	$A_{pancake}$ (nm^2)	A_{brush} (nm^2)
mixture at pH 10.0	429	137
mixture at pH 5.7	540	137
mixture at pH 2.5	555	145

We thus expect a nonadsorbing block tethered to the surface by the PI block. The surface pressure shows only a small increase with compression. At pH 5.7, the carboxyl acid groups of PAA chains are partially ionized, and a small fraction of the PAA chains can absorb at the air−water surface. At pH 2.5, all of the carboxyl groups are protonated, and the neutral PAA chains show increased surface activity. Here, the nonmonotonic increase in surface pressure (at an area per molecule of ∼40 nm^2) is interpreted in previous studies[36,37] as a pancake-to-brush transition.

TABLE 2: Fitted Neutron Reflectivity Parameters for PI_{92}−*b*-PEO_{1290} and Mixtures of PI_{92}−*b*-PEO_{1290}/PI_{63}−*b*-PAA_{530} Monolayers[a]

sample	layer	Nb/10^{-6} (Å^{-2})	ϕ_p	*d* (Å)	Γ (mg/m^2)
PI_{92}−*b*-PEO_{1290}	layer 1	2.34	0.59	15.2	1.02
mixture at pH 10.0	layer 1	2.14	0.75	13.3	1.16
	layer 2	4.7	0.04	62.0	0.29
mixture at pH 5.7	layer 1	3.76	0.27	22.7	0.71
	layer 2	4.54	0.04	129.1	0.60
mixture at pH 2.5	layer 1	1.64	0.89	30	3.1

[a] Nb = scattering length density; ϕ_p = polymer volume fraction; *d* = thickness; Γ = adsorption density.

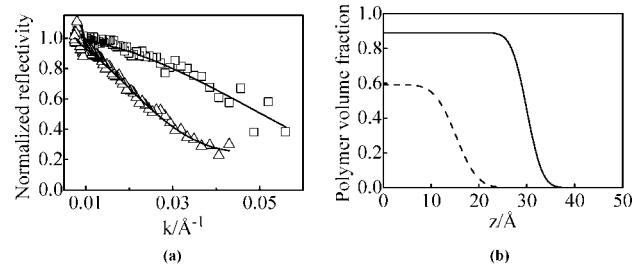

Figure 5. (a) Normalized reflectivity of diblock monolayers at pH = 2.5: PI_{92}−*b*-PEO_{1290} alone (open squares) and PI_{92}−*b*-PEO_{1290}/PI_{63}−*b*-PAA_{530} mixture (open triangles). The solid lines are best-fit curves with corresponding polymer density profiles shown in (b). The measurements are taken in region III, which is indicated by vertical arrows in Figure 4 (pH = 2.5). (b) Corresponding concentration profiles of the PI_{92}−*b*-PEO_{1290} layer (dash line, one-layer model) and the PI_{92}−*b*-PEO_{1290}/PI_{63}−*b*-PAA_{530} layer (solid line, one-layer model).

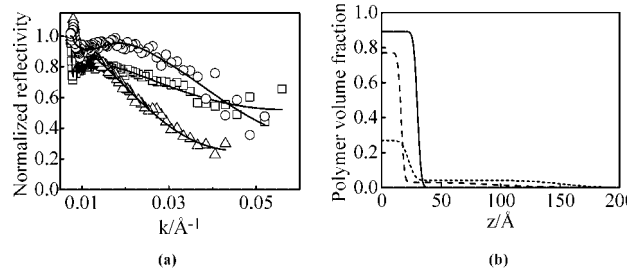

Figure 6. (a) Normalized reflectivity of PI_{92}−*b*-PEO_{1290}/PI_{63}−*b*-PAA_{530} mixed layers on different pH subphases, pH = 2.5 (open triangles), 5.7 (open squares), and 10.0 (open circles). The solid lines are best-fit curves with corresponding polymer density profiles shown in (b). The measurements are taken in region III, indicated by vertical arrows in Figure 4. (b) Corresponding concentration profiles of mixed layers at pH = 2.5 (solid line, one-layer model), 5.7 (dotted line, two-layer model), and 10.0 (dash line, two-layer model).

(iii) PI−b-PEO/PI−b-PAA Mixed Layers. Figure 3 shows surface pressure isotherms for mixtures of PI_{92}−*b*-PEO_{1290}/PI_{63}−*b*-PAA_{530} (molar ratio of EO/AA is ∼1) conducted within the pseudoplateau region (target area per molecule = 110 nm^2) at different pHs. For comparison with the curve for PI_{92}−*b*-PEO_{1290} alone (Figure 1), the surface pressure of the mixture is plotted as a function of the area per PEO molecule. For pH 10.0 and 5.7, the isotherms are similar; the compression−expansion curves show hysteresis similar to that for PI_{92}−*b*-PEO_{1290} alone, and both curves exhibit a pseudoplateau region indicative of immersion of the PEO segments into the subphase. The presence of PAA chains therefore does not appear to influence the monolayer behavior in a significant manner.

At pH 2.5, however, a remarkable difference is obtained. The isotherm is almost linear, with no pseudoplateau within the range of compression. This behavior is interpreted as an effect of hydrogen-bonding complexation between the PAA and PEO.

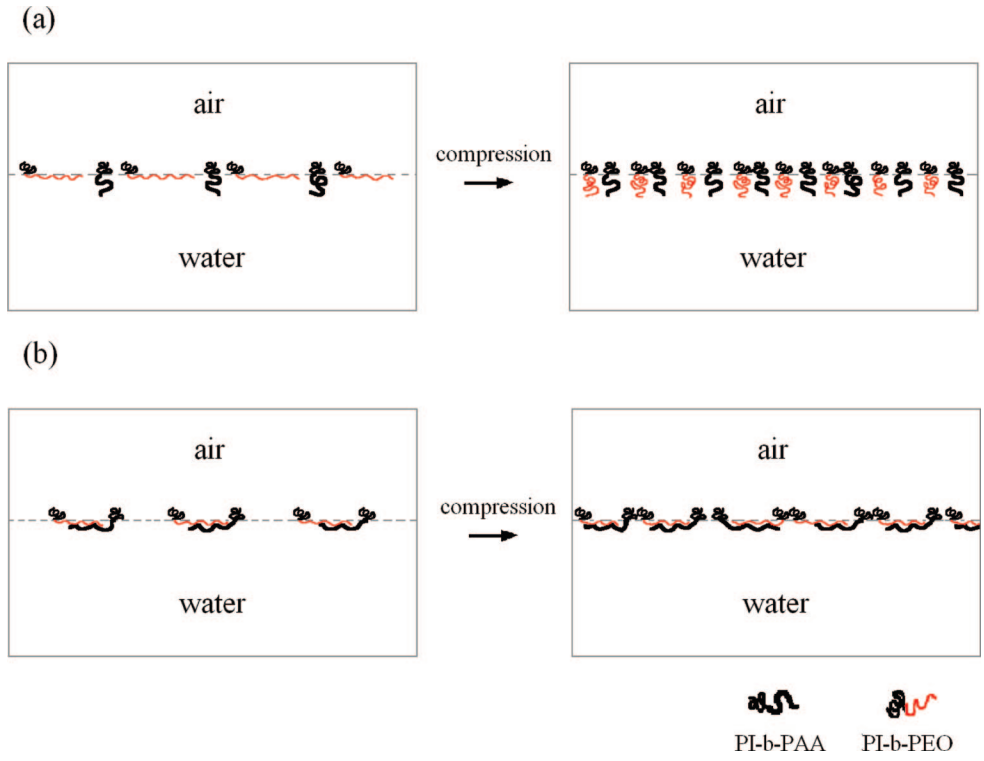

Figure 7. Schematic illustration of the interfacial behavior of $PI_{92}-b-PEO_{1290}/PI_{63}-b-PAA_{530}$ mixed layers; (a) pH > pK_a, (b) pH < pK_a.

Indeed, it has been shown that at molar ratio of EO/AA is ~1, the hydrogen bond density is at its maximum.[38,39] It appears that for the mixed hydrophobic layer thus formed, the PEO segments are prevented from desorbing from the air−water interface; consequently, the pseudoplateau disappears from the compression isotherm. In addition, the compression−expansion cycles overlap, with no sign of hysteresis. This further suggests that in the compressed layer, entanglement of the PEO chains is hindered when they are hydrogen bonded to the PAA chains. Hydrogen bonding between the two polymer species thus produces a mixed surface layer with enhanced stability. For these mixed layers, the limiting pancake areas are $A_{pancake} = 429$, 540, and 555 nm^2 at pH 10.0, 5.7, and 2.5, respectively (Table 1). Here, since the surface pressure is plotted as a function of area per PEO molecule, these increased limiting areas (compared to $PI_{92}-b-PEO_{1290}$ alone, where $A_{pancake} \approx 352.0$ nm^2) are a consequence of the steric effects of the tethered (for pH 10.0) or adsorbed (for pH 2.5) PAA chains.

At higher compression, a third region (III) appears, characterized by a steep rise in surface pressure (Figure 4). For pH 10.0 and 5.7, the rise occurs after the pseudoplateau, and for pH 2.5, it occurs directly from the pancake region (region II is absent). Region III is often considered as the "brush" regime, and extrapolation of this region to $\pi = 0$ mN/m yields the "brush" limiting areas $A_{brush} = 137$, 137, and 145 nm^2 for pH 10.0, 5.7 and 2.5, respectively (Table 1). Surprisingly, unlike the limiting pancake area, these "brush" areas appear to be rather insensitive to pH.

The origin of region III in the $\pi-A$ isotherm is classically attributed to repulsion of the "brush" structures that are formed at high coverage when the intermolecular distance becomes inferior to the radius of gyration of the tethered chain. However, in the case of diblock copolymers where the anchoring block spreads and occupies non-negligible area on the water surface, submerged brush repulsion may not be the sole interpretation for the rapid pressure rise. Indeed, it has been found that for brushes tethered by an anchoring block copolymer, the brush repulsion energies deduced from the surface pressure do not agree well with theoretical predictions.[40] We believe that for this type of system, region III could, depending on the geometry of the diblock, arise primarily from interactions of the anchoring block. In our case, the higher concentration of the anchoring PI blocks in the mixture could be the reason for the appearance of region III since this region is not observed for $PI_{92}-b-PEO_{1290}$ alone at comparable surface coverage expressed in area per PEO molecule. Surface pressure measurements alone, therefore, do not provide reliable information on the structure of the surface layer.

Neutron Reflectivity Measurements. To resolve the structures of the monolayers, in particular in region III, neutron reflectivity (NR) is performed on the compressed layers. Figure 5a shows normalized reflectivity (R/R_F) of $PI_{92}-b-PEO_{1290}$ and of $PI_{92}-b-PEO_{1290}/PI_{63}-b-PAA_{530}$ layers at pH = 2.5 and at an area per molecule of ~50 nm^2 (indicated by vertical arrows in Figure 4). In this normalized representation (R_F is the reflectivity from pure solvent), all deviations of R/R_F from unity are attributed only to the polymer layer. In the contrast scheme used in the present study, in the case of mixed layer, both the PEO and PAA submerged blocks contribute to the reflectivity signal. On the other hand, the signal from the anchoring PI block is negligible since it is almost contrast-matched to air (PI scattering length density ~ 0.26×10^{-6} Å^{-2}), and the spread PI is monomolecularly thin. Thus, as seen in the reflectivity profiles, more polymeric materials are present in the mixed $PI_{92}-b-PEO_{1290}/PI_{63}-b-PAA_{530}$ layer. The solid lines through the experimental points are the best-fit curves calculated using an n-layer step function model with interfacial roughness described by an error function. The scattering length density profile in the direction normal to the interface Nb(z) is given by

$$\mathrm{Nb}(z) = \sum_{n=0}^{N}\left(\frac{\mathrm{Nb}_i - \mathrm{Nb}_{i+1}}{2}\right)\left(1 - \mathrm{erf}\frac{(z - z_i)}{\sigma_i}\right) \quad (1)$$

where Nb_i is the scattering length density and σ_i is the roughness of the layer i.

The reflectivity curves shown in Figure 5 are adequately described by a one-layer model; increasing the number of layers does not improve the quality of fit. From the fitted scattering length density profile Nb(z), the polymer density profile ϕ(z) can be estimated using the relations $\mathrm{Nb_L} = \phi_\mathrm{P}\mathrm{Nb_P} + \phi_\mathrm{S}\mathrm{Nb_S}$ and $\phi_\mathrm{P} + \phi_\mathrm{S} = 1$. $\mathrm{Nb_L}$ is the fitted scattering length density for the layer, $\mathrm{Nb_P}$ and $\mathrm{Nb_S}$ are the scattering length densities of the polymer and the solvent, respectively, and ϕ_P and ϕ_S are the volume fractions of the polymer and solvent in the layer, respectively. For the monolayer of $\mathrm{PI_{92}}-b-\mathrm{PEO_{1290}}$ alone, $\mathrm{Nb_P}$ is taken to be that of PEO, with $\mathrm{Nb_P} \approx 0.64 \times 10^{-6}$ Å^{-2}. For the mixed $\mathrm{PI_{92}}-b-\mathrm{PEO_{1290}}/\mathrm{PI_{63}}-b-\mathrm{PAA_{530}}$ layer, an average for the two polymers PEO and PAA is used, giving $\mathrm{Nb_P} \approx 1.25 \times 10^{-6}$ Å^{-2}, and $\mathrm{Nb_S} \approx 4.8 \times 10^{-6}$ Å^{-2} in all cases. Therefore, in the mixed layer, we do not distinguish between PEO and PAA. The corresponding polymer density profiles thus evaluated are shown in Figure 5b. These density profiles show that in the presence of $\mathrm{PI_{63}}-b-\mathrm{PAA_{530}}$, the total polymer layer is denser and thicker, evidence for the formation of stable mixed layers.

Figure 6a shows normalized reflectivity of the mixture of $\mathrm{PI_{92}}-b-\mathrm{PEO_{1290}}/\mathrm{PI_{63}}-b-\mathrm{PAA_{530}}$ at different pHs, measured at a comparable surface coverage (indicated by the vertical arrow in Figure 4). A strong pH dependence is clearly seen from the increase in the deviation of R/R_F from unity when the pH is decreased from 10.0 to 2.5. The surface layer is thus richer in polymer at lower pH. The corresponding fitted density profiles (Figure 6b) show that the structure of the surface layer also differs under the various pH conditions. At pH = 2.5, the polymer layer, described by a one-layer model, is dense and rich in PEO/PAA complex. At pH = 10.0 and 5.7, however, a two-layer model is required to give the best-fit result. In the two-layer model, the first layer is richer in polymer while and the second layer is very dilute and extends to about 150−200 Å in the subphase. Here, the second extended layer may be interpreted as a signal of brush-like structure. These results reveal that in regime III of the $\pi-A$ isotherms (see Figure 4), brush-like structures are formed at pH 10 and 5.7, where the PAA chains are charged. At pH 2.5, however, the surface layer is dense and compact, and the steep rise in surface pressure cannot be explained by brush formation (in this case, the "A_brush" value given in Table 1 only indicates the limiting area of the pressure rise). Hydrogen-bond complexation of PEO with PAA thus inhibits reorganization of the PEO chains, and upon compression, instead of forming loops and brush-like structures, the PEO chains are strongly bound to the uncharged and surface-active PAA chains. A schematic illustration of the different interfacial behavior of mixed $\mathrm{PI_{92}}-b-\mathrm{PEO_{1290}}/\mathrm{PI_{63}}-b-\mathrm{PAA_{530}}$ layers is shown in Figure 7. The total surface concentration in mg/m^2 can also be evaluated from $\Gamma = \phi_\mathrm{P} d\rho \times 10^{-1}$, where ρ is the density of the polymer, 1.13 and 1.20 g/cm^3 for PEO and PAA, respectively. The fitted parameters and calculated values for each sample are given in Table 2.

Concluding Remarks

Combined surface pressure and neutron reflectivity results show that poly(isoprene)−*b*-poly(ethylene oxide) ($\mathrm{PI_{92}}-b-\mathrm{PEO_{1290}}$) and poly(isoprene)−*b*-poly(acrylic acid) ($\mathrm{PI_{63}}-b-\mathrm{PAA_{530}}$) form mixed monolayers whose interfacial behavior is highly pH-dependent. At pH 10.0 and 5.7, where the carboxyl acid groups are deprotonated, the PAA chains do not appear to induce any unusual effect on the behavior of the PI−*b*-PEO layer. The $\pi-A$ isotherms of the mixture $\mathrm{PI_{92}}-b-\mathrm{PEO_{1290}}/\mathrm{PI_{63}}-b-\mathrm{PAA_{530}}$ exhibit three regions resembling those of PI−*b*-PEO alone, although steric effects of the PAA chains promote the appearance of regime III. In this region of rapid pressure rise, neutron reflectivity measurements confirm the formation of brush-like structures in the tethered layer. At pH 2.5, a novel behavior is observed; the $\pi-A$ isotherm exhibits only two regions, with the disappearance of the pseudoplateau; furthermore, the compression−expansion cycles are completely reversible. These features suggest that desorption of PEO segments and their entanglement are hindered. These results are interpreted in terms of hydrogen-bond complexation between the undissociated carboxylic groups and the PEO. Neutron reflectivity shows that the mixed layers thus formed are thin and compact even up to region III. Thus, the rapid rise in pressure in this region is primarily due to interactions of the anchoring block. Intermolecular complexation through hydrogen bonding thus provides a potential route to densification and increased stability of surface monolayers that may be of interest in practical systems.

Acknowledgment. The financial support of Ministry of Science and Technology of China (2007CB936401) is acknowledged. D.X. thanks the China Scholarship Council for the scholarship to stay in France. We thank F. Cousin and A. Menelle for help with the reflectometer.

References and Notes

(1) Alexander, S. *J. Phys. (Paris)* **1977**, *38*, 983–987.
(2) de Gennes, P. G. *Macromolecules* **1980**, *13*, 1069–1075.
(3) Halperin, A. *J. Macromol. Sci.* **1992**, *A-29*, 107–116.
(4) Ligoure, C. *J. Phys. II* **1993**, *3*, 1607–1617.
(5) Carignano, M. A.; Szleifer, I. *Macromolecules* **1995**, *28*, 3197–3204.
(6) Szleifer, I. *Europhys. Lett.* **1998**, *44*, 721–727.
(7) Milner, S. T. *Science* **1991**, *251*, 905–914.
(8) Halperin, A.; Tirrell, M.; Lodge, T. P. *Adv. Polym. Sci.* **1992**, *100*, 31–71.
(9) Balazs, A. C.; Singh, C.; Zhulina, E.; Chern, S. S.; Lyatskaya, Y.; Pickett, G. *Prog. Surf. Sci.* **1997**, *55*, 181–269.
(10) Zhao, B.; Brittain, W. J. *Prog. Polym. Sci.* **2000**, *25*, 677–710.
(11) Currie, E. P. K.; Norde, W.; Cohen Stuart, M. A. *Adv. Colloid Interface Sci.* **2003**, *100−102*, 205–265.
(12) Rühe, J.; Ballauff, M.; Biesalski, M.; Dziezok, P.; Gröhn, F.; Johannsmann, D.; Houbenov, N.; Hugenberg, N.; Konradi, R.; Minko, S.; Motornov.; Netz, R. R.; Schmidt, M.; Seidel, C.; Stamm, M.; Stephan, T.; Usov, D.; Zhang, H. N. *Adv. Polym. Sci.* **2004**, *165*, 79–150.
(13) Toomey, R.; Tirrell, M. *Annu. Rev. Phys. Chem.* **2008**, *59*, 493–517.
(14) Bijsterbosch, H. D.; de Haan, V. O.; de Graaf, A. W.; Mellema, M.; Leermakers, F. A. M.; Cohen Stuart, M. A.; van Well, A. A. *Langmuir* **1995**, *11*, 4467–4473.
(15) Gonçalves da Silva, A. M.; Filipe, E. J. M.; d'Oliveira, J. M. R.; Martinho, J. M. G. *Langmuir* **1996**, *12*, 1647–6553.
(16) Gonçalves da Silva, A. M.; Simões Gamboa, A. L.; Martinho, J. M. G. *Langmuir* **1998**, *14*, 5327–5330.
(17) Dewhust, P. F.; Lovell, M. R.; Jones, J. L.; Richards, R. W.; Webster, J. R. P. *Macromolecules* **1998**, *31*, 7851–7864.
(18) Gragson, D. E.; Jensen, J. M.; Baker, S. M. *Langmuir* **1999**, *15*, 6127–6131.
(19) Fauré, M. C.; Bassereau, P.; Lee, L. T.; Menelle, A.; Lheveder, C. *Macromolecules* **1999**, *32*, 8538–8550.
(20) Cox, J. K.; Yu, K.; Eisenberg, A.; Lennox, R. B. *Phys. Chem. Chem. Phys.* **1999**, *1*, 4417–4421.
(21) Baker, S. M.; Leach, K. A.; Devereaux, C. E.; Gragson, D. E. *Macromolecules* **2000**, *33*, 5432–5436.
(22) Noskov, B. A.; Akentiev, A. V.; Miller, R. *J. Colloid Interface Sci.* **2002**, *247*, 117–124.
(23) Rivillon, S.; Muñoz, M. G.; Monroy, F.; Ortega, F.; Rubio, R. G. *Macromolecules* **2003**, *36*, 4068–4077.
(24) Tsukanova, V.; Salesse, C. *Macromolecules* **2003**, *36*, 7227–7235.

(25) Hosoi, A. E.; Kogan, D.; Devereaux, C. E.; Bernoff, A. J.; Baker, S. M. *Phys. Rev. Lett.* **2005**, *95*, 037801.
(26) Logan, J. L.; Masse, P.; Gnanou, Y.; Taton, D.; Duran, R. S. *Langmuir* **2005**, *21*, 7380–7389.
(27) Cheyne, R. B.; Moffitt, M. G. *Langmuir* **2006**, *22*, 8387–8396.
(28) Jiang, M.; Li, M.; Xiang, M.; Zhou, H. *Adv. Polym. Sci.* **1999**, *146*, 121–196.
(29) Niwa, M.; Hayashi, T.; Higashi, N. *Langmuir* **1990**, *6*, 263–268.
(30) Yan, X.; Janout, V.; Hsu, J. T.; Regen, S. L. *J. Am. Chem. Soc.* **2003**, *125*, 8094–8095.
(31) Mccullough, D. H., III; Regen, S. L. *Chem. Commun.* **2004**, 2787–2791.
(32) Li, J. W.; Janout, V.; Mccullough, D. H., III; Hsu, J. T.; Truong, Q.; Wilusz, E.; Regen, S. L. *Langmuir* **2004**, *20*, 8214–8219.
(33) Mccullough, D. H., III; Grygorash, R.; Hsu, J. T.; Regen, S. L. *J. Am. Chem. Soc.* **2007**, *129*, 8663–8667.
(34) Lopes, S. I. C.; Gonçalves da Silva, A. M. P. S.; Brogueira, P.; Piçarra, S.; Martinho, J. M. G. *Langmuir* **2007**, *23*, 9310–9319.
(35) Hadjichristidis, N.; Pispas, S.; Floudas, G. *Block Copolymers: Synthetic Strategies, Physical Properties and Application*; John Wiley & Sons, Inc.: Hoboken, NJ, 2003.
(36) Currie, E. P. K.; Sieval, A. B.; Fleer, G. J.; Cohen Stuart, M. A. *Langmuir* **2000**, *16*, 8324–8333.
(37) Joncheray, T.; Bernard, S. A.; Matmour, R.; Lepoittevin, B.; El-Khouri, R. J.; Taton, D.; Gnanou, Y.; Duran, R. S. *Langmuir* **2007**, *23*, 2531–2538.
(38) Xie, D. H.; Xu, K.; Bai, R. K.; Zhang, G. Z. *J. Phys. Chem. B* **2007**, *111*, 778–781.
(39) Xie, D. H.; Bai, W.; Xu, K.; Bai, R. K.; Zhang, G. Z. *J. Phys. Chem. B* **2007**, *111*, 8034–8037.
(40) Kent, M. S.; Lee, L. T.; Factor, B. J.; Rondelez, F.; Smith, G. S. *J. Chem. Phys.* **1995**, *103*, 2320–2342.

JP808821S